DOI: 10.13009/EUCASS2017-279

Numerical simulation and measurements of wall heat fluxes in a single-element GO2/GCH4 rocket combustor

Ye Hong[1], Zhanyi Liu[2], Simona Silvestri[1], Maria P. Celano[1], Oskar J. Haidn[1], Zhendong Yu[1]

[1] Institute of Turbomachinery and Flight Propulsion, TU München, 85748 Garching, Germany

[2]Science and Technology on Liquid Rocket Engine Laboratory, Xi'an Aerospace Propulsion Institute, 289 Feitian Road, Aerospace Base, Xi'an, Shaanxi Province, China

Abstract

A rocket combustion chamber with a single coaxial shear injector is tested. The hot firing tests are conducted with gaseous methane and gaseous oxygen at a mass ratio of oxidizer to fuel of 2.647 and at a pressure of 2 MPa. Wall temperatures are measured along the axis of the chamber and the wall heat fluxes are calculated based on inverse heat conduction approach. To better analyze the experimental results, numerical simulations are performed applying the commercial CFD code ANSYS Fluent. The eddy dissipation concept model is adopted to model turbulent combustion. Mesh independency studies have been performed prior to any further analyses. The ultimate target is to compare the heat fluxes obtained from simulation with the experimental data. Hot gas temperature distribution and flow field structures are also investigated for a better understanding of the experimentally determined heat flux profile. The comparison demonstrates that the simulation approach followed is capable to predict wall heat fluxes in a rocket combustor with sufficient accuracy.

1. Introduction

Nowadays, three propellant combinations are mostly utilized in high performance liquid propellant rocket engines. These are liquid oxygen/liquid hydrogen (LOX/LH2), unsymmetrical dimethyl-hydrazine/nitrogen-tetroxide (UDMH/NTO) and LOX/kerosene. The advantage of LOX/LH2 is the highest specific impulse among the three, while LH2's low density and extremely low boiling point mean bigger tank and being not storable. The hypergolic and storable nature are the most attractive characteristics of UDMH/NTO but its toxicity related handling problems and pollution issues together with the rather poor performance make this propellant combination less and less acceptable, especially in modern societies. Therefore, as a compromise, LOX/kerosene has been used in rocket propulsion for decades because of its relatively low cost, low pollution and high performance. Many famous LOX/kerosene rocket engines, such F-1, NK-33, RD-180, were designed, manufactured and applied successfully in United States and the former Soviet Union. Even today, Falcon 9, ATLAS 5, Zenit 2/3 and Soyuz rockets are flying LOX/kerosene rocket engines.

Although kerosene has some disadvantages in comparison to methane it is still an important fuel in present liquid rockets. Firstly, the coking temperature of kerosene on the hot gas-side of the liner walls is the main limitation for the use in the regenerative cooling system which prevails in large thrust liquid rocket engines. Hence, almost all high pressure kerosene/oxygen engines apply some sort of film cooling in order to manage the high heat loads and stay within the coking limits. For pure methane instead, the widely quoted coking temperature is 970K and thus much higher than that of kerosene (590K) [1]. Secondly, methane provides not only a better specific impulse but an improved heat transfer performance because of its high thermal conductivity, specific heat and low viscosity [2]. In summary, from a system point of view [3], methane could despite its lower density which yields larger propellant tanks be a promising fuel as a propellant for reusable rocket engine, which has already been a concern for rocket engineers.

Actually, some researches about this propellant combination oxygen/methane have been conducted in some projects of the United States [4], Europe [5], [6], Japan [7] and Russia [8]. However, until now no oxygen/methane rocket engine is flying yet. There are still unresolved issues between the fundamental research and technology development and a final practical application and detailed knowledge about heat transfer characteristics in such combustion chambers is one of the most important. Additionally, the continuously growing pressure for cost reduction has forced the aerospace industry to cut down trial and error approaches as much as possible which go along with expensive experimental testing programs and rely more and more on advanced numerical design tools. Therefore, the numerical simulation has been combined in our effort with experimental results to investigate key phenomena occurring in combustion chamber. Such an approach has been shown to yield successful results for oxygen/hydrogen combustion [9] [10] [11].

As already mentioned before, the combustion chamber is one of the most important components of a liquid propellant rocket engine. The axial distribution of the heat release has an enormous impact on the local wall heat loads and finally

DOI: 10.13009/EUCASS2017-279

on the distribution of the hot-gas side wall temperatures, the required local cooling and the final structural lifetime expectation. The importance of these local heat flux and wall temperature data is confirmed by the fact that life cycle predictions of rocket engine liners strongly depend on the accuracy of the wall temperatures and where an error of 40 K may lead to 50% life reduction in a cryogenic propellant rocket chamber [12].
In this paper, the wall heat flux measurements in a GO2/GCH4 single element combustion chamber and corresponding numerical simulation investigation are conducted. This paper comprises four parts. The experimental facilities and setup are described briefly first. Then the detailed approach to obtain the wall heat flux from the temperature data is introduced. The third part provides a brief description of the numerical simulation method and the final fourth part is dedicated to the comparison between the modeling and testing results.

2. Experimental methods and data processing

The experiments have been carried out in the Institute of Flight Propulsion's Lab at the Technical University of Munich. The test rig comprises a coaxial shear injector, a square combustion chamber and a nozzle. The nozzle has a throat with a rectangular cross section. The rig features a contraction ratio of 2.5 which yields a Mach number of 0.25 similar to real rocket engines conditions. The single coaxial injector is flush mounted to the chamber faceplate. The dimensions of the chamber and injector are shown in Table 1. It is worthwhile mentioning that with an absolute value of 3mm, the injector / wall distance is rather small. Gaseous oxygen at 278K enters the combustion chamber from the inner channel of the injector and gaseous methane at 269K enters from the outer channel. Sonic orifices are used to determine the inlet mass flow rates. The mass flow of oxygen is 45g/s and the parameter of methane is 17g/s. The combustion chamber with the length of 290mm has no cooling measures and therefore the burning time is limited to a few seconds only. The material used for the chamber segment and the nozzle segment is oxygen-free copper (Cu-HCP). The nozzle is designed to control the chamber pressure. With the mass flow rate given above and the throat area the nominal chamber pressure is set to 2 MPa. Due to the cooling type of the chamber, the run time is 3s and thus the heat conduction in the solid is inherently transient. The operating condition of the test case is shown in Table 2.

Table 1: Dimensions of combustion chamber and injector

Combustion chamber		Injector	
Chamber length	290mm	GO2 diameter	4mm
Chamber width	12mm	GO2 post thickness	0.5mm
Chamber height	12mm	GO2 post recess	0mm
Throat height	4.8mm	GCH4 outer diameter	6mm

Table 2: Operating condition of the test case

	GO2	GCH4
Inlet mass flow(g/s)	45	17
Inlet temperature(K)	278	269
Nominal chamber pressure(MPa)	2	
Nominal oxidizer to fuel ratio	2.647	

Seventeen thermocouples are located along the axial direction with a regular path of 17mm on the upper side of the chamber. The first thermocouple is located on the axial position of faceplate. All the seventeen thermocouples are located within the chamber wall with 1mm distance to the hot wall. In addition, multiple pressure transducers measure the combustion pressure along the chamber axis. More detailed information about the test rig can be found in reference [13].
The heat fluxes in the combustion chamber are obtained from the temperature data provided by thermocouples applying an inverse heat conduction method. The ignition moment is defined as t=0 s. The initial temperature distribution of the entire combustion chamber is obtained by performing an extrapolation of the measured values of the discrete thermocouples. Then a heat flux profile along the axis should be guessed to initiate the calculation. With the initial and boundary conditions defined, the temperature field of the chamber is obtained at the following time step. At this moment, a comparison between the computed and measured values of the temperature at the thermocouple locations is performed. The wall heat flux profile will be modified at each iteration step until the square root of the sum of the quadratic temperature differences fulfils a predefined minimum. The predicted temperature field can then be regarded as the initial condition for next time step and a new heat flux profile should be guessed once again for the next time step. Analogously, the heat flux profiles can be acquired at each time step. It is necessary to mention that an averaged

DOI: 10.13009/EUCASS2017-279

heat flux at each axial position is used in the reconstruction process due to the lack of thermocouples at different circumferential positions.

Actually, for each time step, it is a multiple targets tracking problem and the targets are heat fluxes at each axial position. A robust calculation should be able to converge independently of the initial condition, however a prediction of the heat flux profile close to the actual value, can speed up the convergence. To get more exact results, it is necessary to consider the longitudinal heat conduction, that is why the multiple targets tracking problem appears. But if the longitudinal heat conduction is ignored, it will become a single target tracking problem for each axial position, which is easier to solve. Moreover, the results from the simpler problem can be regarded as the preset heat flux profile for each time step, which are believed to be closer to the actual values than randomly guessed ones. Since the cross section of the chamber wall is rectangular, the calculation is two-dimensional when the longitudinal heat conduction is ignored. The label '2d' will be used to represent this case and '3d' represents the other case where longitudinal heat conduction is considered.

Figure 1 presents the heat flux profiles along the axial direction (z) for the cases 2d and 3d at several different moments in time. Z=0 mm denotes the axial position of the faceplate. It is shown that the heat fluxes vary with z in the similar trend at each moment, but there is slight difference between the values for the 2d and 3d case. Nevertheless, the results for the 2d case are still acceptable, especially for a preliminary analysis since they require much less computing time compared to the 3d case.

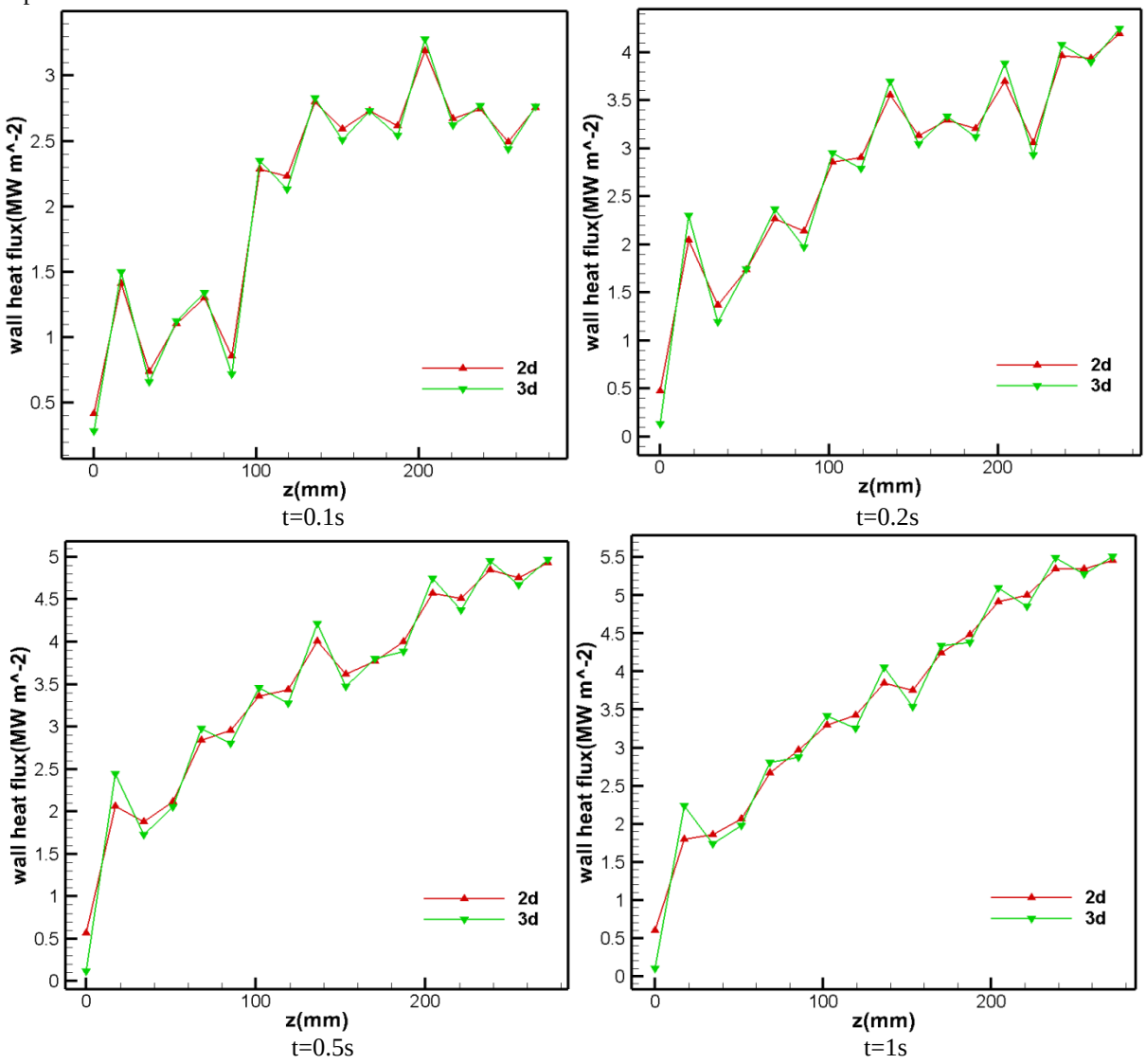

DOI: 10.13009/EUCASS2017-279

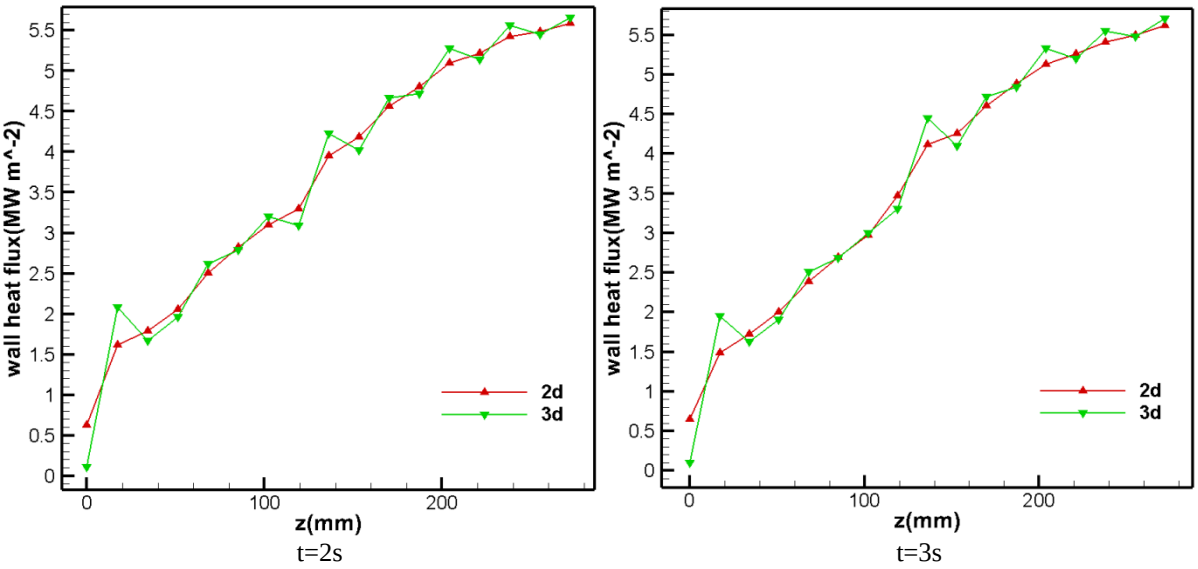

Figure 1: Comparison of heat flux profiles for 2d and 3d cases at different time steps

In the heat flux calculation, the thermal characteristics of the material Cu-HCP, which are reported in Table 3, are cited from German Copper Institute [14].

Table 3: Thermal characteristics of Cu-HCP

Density	8940 kg/m^3
Thermal conductivity	385 W/m/K
Temperature(K)	Specific heat(J/kg/K)
293	385
373	393
473	403

Figure 2 presents the temporal behavior of the heat fluxes at each axial position. While for the front part of the chamber ($z \leq 102$mm) the heat fluxes show a rather steep increase at the beginning of the test for the first 200ms followed by a further but less steep increase until a peak value is reached between additional 200 - 300ms and then the fluxes show a slight decrease subsequently, the behavior in the rear part ($z \geq 153$mm) of the chamber is entirely different. Here the predicted heat fluxes show as well a steep increase for the first 100 - 200ms followed by range where the increase is gradually reduced until, depending on the axial position, a plateau value can be identified. Obviously, there is an intermediate region where the heat flux profiles show both of the features mentioned previously.

At the beginning of the test, the chemical reactions generate through the heat release a sudden increase of the gas temperature in the chamber and a subsequent increase of the wall temperatures and the wall heat fluxes. With the time passing, the inner surface temperature increases and thus the temperature differences between the gas in the wall boundary layer and the wall surface decreases. In the front part, the gas temperatures are lower due to the incomplete combustion. Hence, after the sudden increase in the very beginning any further changes of the temperatures are relatively small and this behavior dominates the variation of the heat fluxes in this region. In the rear part we have at least two effects which influence the wall heat loads. Although we have a continuously accelerated flow due to the heat release, there will be a relatively cool boundary layer due to the heat losses in the front part of the combustion chamber. However, at those downstream positions most of the heat release has already taken place and the hot gas temperatures have reached almost equilibrium conditions (>3000K). As a consequence of this negligible heat loss a more stable boundary layer establishes and subsequently the heat fluxes tend towards constant values. From the reconstruction of the chamber temperature field, it is found that the temperature of the inner surface increases by no more than 70K after 1s, which does not have significant impact on the heat flux, so a flat trend shows up after 1s. Additionally, the longitudinal heat conduction from the rear part to the front part is also a favorable factor for the analysis.

DOI: 10.13009/EUCASS2017-279

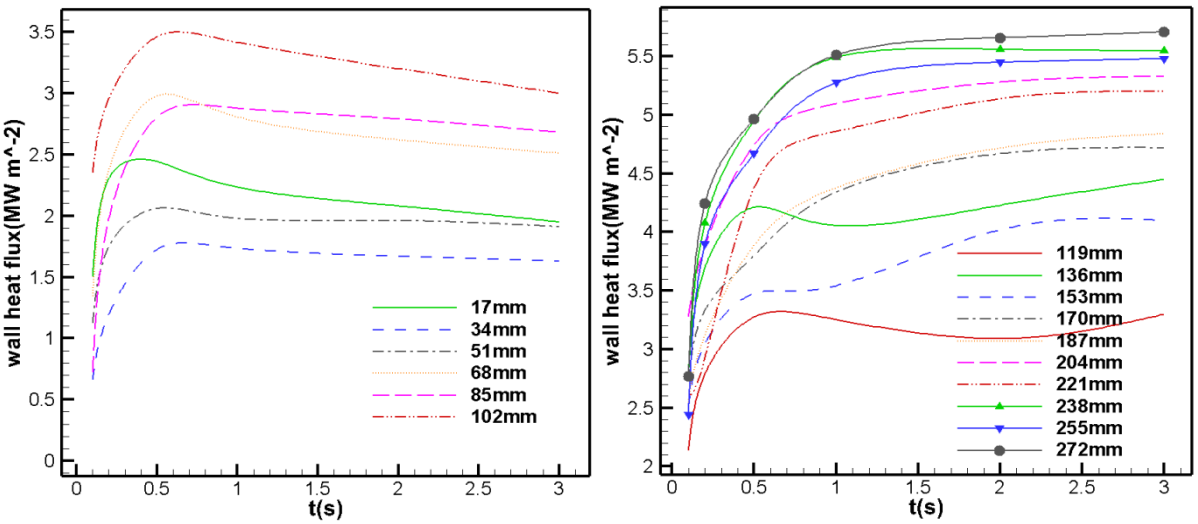

front part rear part

Figure 2: Heat fluxes vary with time at each axial position

In order to validate the numerical simulation approach and to provide additional information about flow and temperature field development inside the combustion chamber, simulations about this test case have been conducted in which the inner surface temperature profile at 3s has been applied as the temperature boundary condition. Figure 3 presents the inner surface temperature distribution along the axial direction at 3s for the 3d case where the temperature distributions of upper surface and side surface are shown respectively, which takes into account the effect due to different thickness of combustion chamber walls, too.

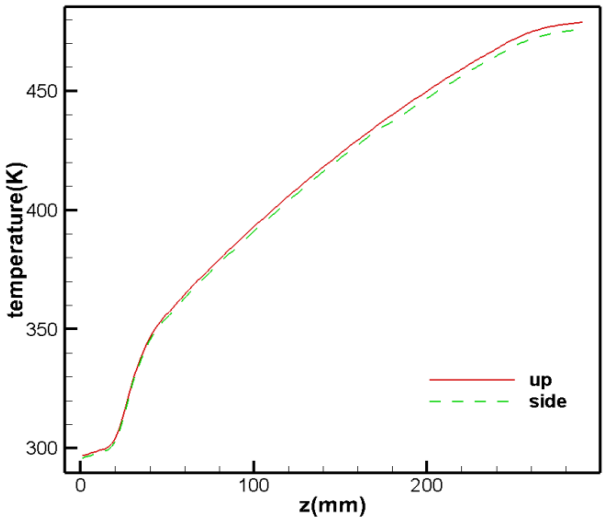

Figure 3: Axial wall surface temperature profile at 3s

3. Numerical simulation approach

The simulations are performed applying ANSYS Fluent, a finite volume based method. Many research institutes have made great effort to perform reliable numerical simulations of gas-gas combustion flows and their research has indicated that steady Reynolds averaged Navier-Stokes (RANS) method combined with appropriate chemical kinetic and turbulence modelling is an effective way to model such combustion chamber flows and predict heat fluxes which are in good agreement with experimental results [15] [16] [17] [18] [19] [20].

a. Computational domain

A three-dimensional computational domain is used for the present simulations. The reasons for this approach are, first, previous research indicated that for wall heat flux predictions, a 3D treatment is necessary since a 2D axisymmetric domain has inherent shortcomings [21]. Moreover, the cross section of present chamber is quadrate, and therefore a 2D approach neglects to a large extent 3D effects in the corners. The computational domain chosen includes the combustion chamber, the nozzle and, in order to obtain more accurate injection status, the 80mm long channels of

DOI: 10.13009/EUCASS2017-279

propellants, too. Considering the expensive cost, the computational domain is simplified to a quarter of the chamber, where symmetry boundary conditions are imposed at the cut planes. Fig.4 provides the outline of the computational domain and the view is compressed by a factor of 0.2 in the z-direction.

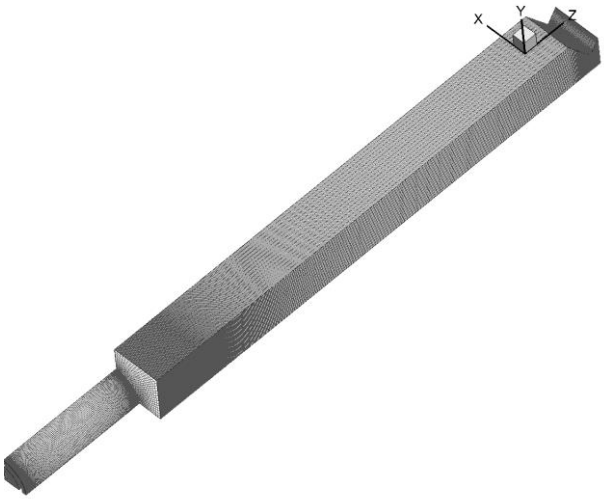

Figure 4: Computational domain

b. Turbulence and combustion model

The classical standard k-ε model is used to model turbulence. The turbulent transport is modelled with the turbulent Schmidt number of 0.7. This value is recommended for high-Reynolds-number jet flows by Yimer [22]. The turbulent Prandtl number is set to the value of 0.85. The description of the turbulence-chemistry interactions represents one of the most difficult tasks in turbulent combustion. It is necessary to adopt a robust model that accounts for both the chemical reactions and the turbulence such as the eddy dissipation concept (EDC) approach, which is possible to consider the detailed chemical dynamic process. In present case, a reduced chemical mechanism with 14 species and 18 reactions is adopted [23].

c. Thermodynamics model

In this simulation, the ideal gas equation of state is utilized for the closure of governing equations, which is reasonable for present pressures and temperatures in the chamber.

d. Wall treatment

Cells in wall boundary layer play a crucial role in the flow field prediction. The meshes in the vicinity of the wall should be very dense. In present simulation, enhanced wall treatment is used to enable the near-wall region to be resolved all the way down to the wall, which is important for heat transfer prediction [24]. Meshes have near-wall resolutions of $y+ \leq 1$.

e. Mesh verification

It is essential to perform mesh convergence studies to gain a mesh-independent solution. In this work, the mesh study is conducted by a successive refinement of the mesh following Richardson's Extrapolation Method [25]. By this mean, to verify the discretization method, eddy-dissipation model with temperature limited to 3700 K and adiabatic wall boundary conditions are used, because of simplicity. A scalar ϕ is approximated with

$$\phi_0 \cong \phi_1 + (\phi_1 - \phi_2)/(r_{1,2}^{\vartheta} - 1) \quad \textbf{(1)}$$

Here ϕ_1 and ϕ_2 represent the simulation results from the fine and middle grids (refinement wise), $r_{1,2}$ represents the grid refinement ratio, and ϑ represents the observed order of grid convergence. ϑ is affected by the spatial discretization method. In the respect of three grids for a three-dimensional domain with decreasing numbers of cells (fine, middle and coarse), the grid refinment ratio $r_{1,2}$ is expressed as

DOI: 10.13009/EUCASS2017-279

$$r_{1,2} = [(\#\text{ of cells of the finest grid})/(\#\text{ of cells of the intermediate grid})]^{1/3} \quad \textbf{(2)}$$

By solving the following equation iteratively, the observed order of convergence ϑ is computed.

$$\varepsilon_{2,3}\%/(r_{2,3}^{\vartheta}-1) = r_{1,2}^{\vartheta}\left[\varepsilon_{1,2}\%/(r_{1,2}^{\vartheta}-1)\right] \quad \textbf{(3)}$$

Here "3" represents the coarse grid and the Richardson Error Estimator $\varepsilon_{n,n+1}$ is given by

$$\varepsilon_{n,n+1}\% = 100(\phi_{n+1}-\phi_n)/\phi_n \quad \textbf{(4)}$$

Here n=[1,2,3] represents the fine, middle and coarse grids. The GCI (grid convergence index) is obtained by

$$GCI_{1,2}\% = F_S\left|\varepsilon_{1,2}\%\right|/(r_{1,2}^{\vartheta}-1) \quad \textbf{(5)}$$

Here F_s represents the factor of safety, which is set to 1.25. Furthermore, α is expressed as

$$\alpha = GCI_{2,3}\%/GCI_{1,2}\% \quad \textbf{(6)}$$

When $\alpha/r_{1,2}^{\vartheta} \approx 1$, the asymptotic value ϕ_0 is recognized as grid independent. The ϕ in equation (1) is the static pressure at the point x,y,z (3mm, 3mm, 250mm). The results in Table 4 shows that the grids are inside the asymptotic convergence region, because $\alpha/r_{1,2}^{\vartheta} \approx 1$. Besides, the observed order of convergence is $\vartheta \approx 2$, which indicates second-order accuracy of discretization in space. Moreover, the uncertainty of ϕ is 0.12% for the fine grid, and 0.05% for middle grid. All the following results have been achieved applying the middle grid.

Table 4: Results of uncertainty verification and grid independency

Grid n	# of Cells	ϕ (p at point) (Pa)	$r_{1,2}$	1.4513	ϑ	2.082
1	7269708	1763200	$r_{2,3}$	1.4133	ϕ_0 (Pa)	1763968
2	2378004	1762300	$GCI_{1,2}\%$	0.05	$\alpha/r_{1,2}^{\vartheta}$	1.000803
3	842447	1760540	$GCI_{2,3}\%$	0.12		

4. Results and discussion

In the following, the results of the numerical simulation and the comparison between experiment and modelling are presented and discussed, beginning with the flame structure and the combustion processes.
The total temperature distribution in a plane perpendicular to the injection faceplate is shown in Fig.6. There is a hot zone existing in the recirculation area of the post tip. The hot zone is the source of the flame which provides for flame anchoring at the post tip and downstream of it, the reaction zone expands gradually. The flame is characterized by a rather moderate broadening of the reacting shear layer which approaches the combustion chamber wall rather slowly which helps to establish a thin low temperature boundary layer. But as the central hot gas gets closer to the wall, this

DOI: 10.13009/EUCASS2017-279

low temperature layer shrinks to a roughly constant thickness from z=150mm on downstream. Additionally, the flame seems to spread rather quickly towards the walls which indicates a strong recirculation area which stretches only a few centimetres downstream. This flow behaviour results in both, a heat flux peak and a wall pressure peak. Obviously, the entire evolution of flame behaviour and wall boundary layer will have an influence on the local wall heat fluxes. Furthermore, the adiabatic flame temperature at equilibrium state calculated based on CEA[26] is 3458 K. This value varies slightly depending on the thermodynamic data used and the product species included. It is a good indicator of the maximum temperature that can occur in a combustion process. The maximum temperature in the present view is 3465.55K, which is close to the equilibrium temperature.

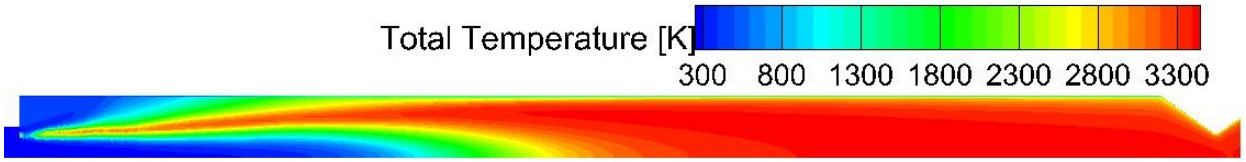

Figure 6: Total temperature distribution in the combustion chamber

A comparison of experimental and numerical heat flux results are shown in Fig.7. As mentioned in the data processing part, the experimentally determined heat flux at each axial position is an averaged one, and therefore the results from the simulation presented here are also averaged in circumferential direction [27]. In the test data, a steep rise shows at the beginning of the chamber, then after a slightly decrease, a gradual ascent trend appears, followed by a relatively flat trend in the rear part of the combustor. As for the simulation result, in general, it evolves in the similar trend with experimental one. Especially, it captures the peak at the beginning and the position of the peak is very close to the test data. The defect is the peak heat flux value deviates from the experimental one. Besides, the heat flux becomes much higher than the experiment from 70mm, peaking up at almost 8 MW/m^2 at 170mm. Definitely, simulation result predicts a lot more heat flux than the experiment. This problem also appears in others' work, probably because of the mesh [27]. Without sufficient boundary layers providing smooth transition, the central hot gas gets closer to the chamber wall, resulting in higher heat flux. Another influence could come from the insufficient species of the chemical mechanism. It is supposed that the chemical scheme has great effect on the mixture heat conductivity and potential low-activation energy reactions [28].

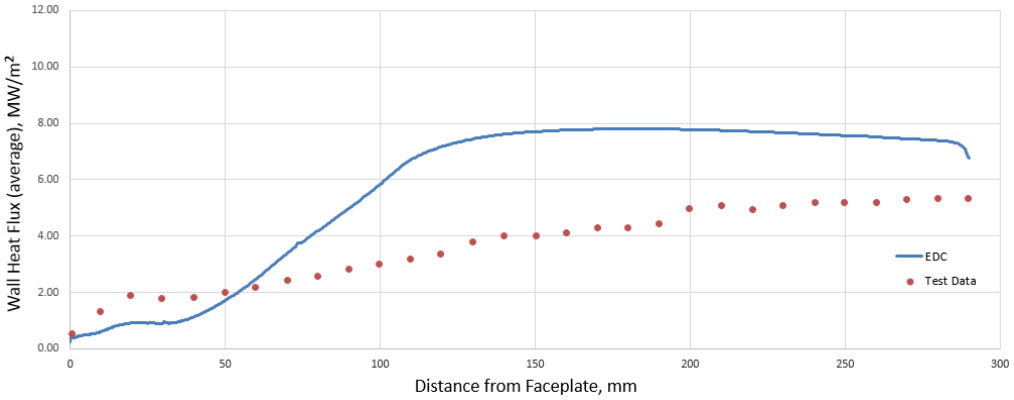

Figure 7: Heat flux averaged along circumference

In addition to heat flux profiles, the experimental data for pressure distribution is also available which allows for a different type of quantitative comparison between test and simulation. Generally, the axial wall pressure profile can be considered a footprint of the axial distribution of the heat release. Heat addition due to the chemical reaction yields an acceleration of the flow and as a result a quadratic shape of the wall pressure decrease. As soon as combustion is complete, the decline of the wall pressure should be constant. Figure.8 illustrates the measured pressure distribution, one β-PDF simulation result from [27] and EDC model's pressure distribution in axial direction. From the experimental data, it can be seen that a sudden rise occurs close to the injector, which is followed by a descent at a decline which at the end of the chamber tends to flatten out. In general, the simulation underestimates the pressure along the whole chamber. Besides, simulation result drops deeper than the experiment from 70mm to 170 mm. As the steeper increase of heat flux in this region, this deviate pressure drop is presumed to be because of coarse mesh. Compared to β-PDF simulation result from [27], computation result with EDC model has closer result to the experiment. Based on this, the EDC model may have some advantages than the β-PDF model, such as, in pressure estimation because of the better prediction of the interaction between the turbulence and reaction.

DOI: 10.13009/EUCASS2017-279

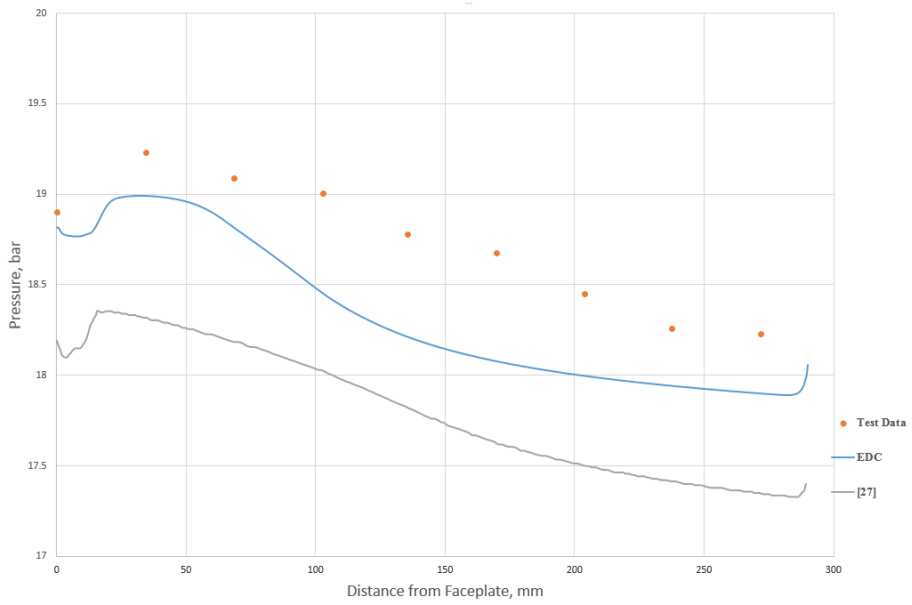

Figure 8: Predicted pressure distribution in the combustor

For a better understanding of the combustion details, the mass fraction of oxygen, which is mass flow averaged, is shown in figure 9. Computational result of a β-PDF model [27] is also shown. The residual value of mass fraction of oxygen at the outlet calculated by CEA is 0.4% [27]. Theoretically, the combustion process is dominated by both the mixing process and the velocity of the chemical reaction, and in particular by the slower one from them. At the beginning of a non-premixed combustion, the oxygen consumption is slow because of the low temperature and low mixing of propellants. As the temperature increases, the chemical reaction rate rises significantly. During the mixing, contact area between the oxygen and fuel expands, which also corresponds to higher oxygen consumption rate. Within a certain temperature region, the reaction rate could be considered infinite. In other words, above a temperature, the combustion is mainly dominated by mixture process. Simulation with EDC model clearly shows this process. In the inlet region, non-premixed combustion occurs only in the interface between the methane and oxygen, which is both influenced by the turbulence flow and chemical reaction. As the propellants mix homogeneously and temperature rises up, the consumption of oxygen accelerates. Undoubtedly, from the EDC model result, the oxygen mass fraction drops a little faster within the region of 70mm-170mm, which is also reflected in the pressure and heat flux result. This drop is presumed to be because of mesh density.

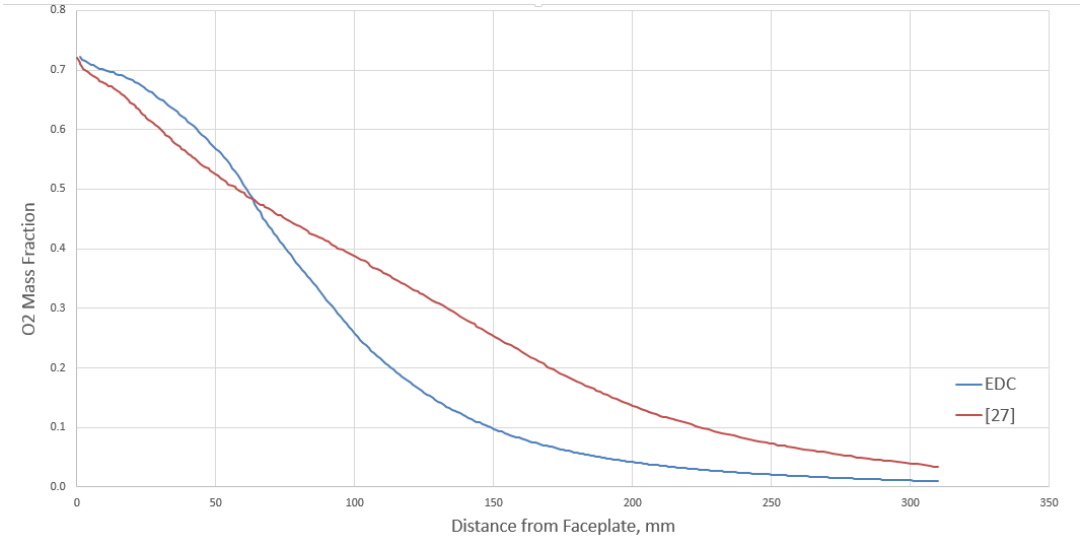

Figure 9: Mass fraction of oxygen mass flow averaged over each cross section along the combustor axis

DOI: 10.13009/EUCASS2017-279

5. Conclusions

In present work, based on a single-element GO2/GCH4 combustor test case conducted in Institute of Turbomachinery and Flight Propulsion of Technical University of Munich, wall heat fluxes have been obtained in terms applying an inverse heat conduction method while flow and combustion processes in the combustor have been simulated using ANSYS Fluent to predict the wall heat flux and wall pressure profile for a comparison with the test data. The interaction between the turbulence and chemical reaction was considered by adopting the eddy dissipation concept model. In general, it can be concluded that the current simulation is able to predict the flow and combustion process to some extent in terms of the comparison of the two typical rocket design parameters, i.e., wall heat flux as well as chamber pressure. Nevertheless, the simulation result has some discrepancy with the test data quantitatively, either on heat flux or chamber pressure. The reasons are twofold. Firstly, in the test rig, no more thermocouples are equipped in the circumferential direction at each axial position, which leads to the lack of more detailed heat flux distribution at each cross section. Secondly, in present simulation, mesh density and reaction mechanism both have an effect on the computation result. With finer mesh and more complexity mechanism, the heat flux should be lower. Although a comparable simulation result is yielded with the current approach, it is necessary to notice that the chamber wall boundary is imposed with a temperature profile obtained from the test data. In principle, to a given issue, simulation should be independent of any experimental data. However, in that case, the solid enclosing the chamber must be conjugated to the current computational domain and a coupled simulation should be performed, which adds greatly to the complexity of the simulation. This simulation approach could be used in the further research of GO2/GCH4 rocket combustor.

Acknowledgements

The authors gratefully acknowledge Institute of Turbomachinery and Flight Propulsion for providing the test case and supercomputer center for numerical simulation. In addition, the first author and second author thank for the financial support from China Scholarship Council. Valuable discussions with Professor Wei Xianggeng are also greatly appreciated.
Part of the work presented in this paper has been funded by the German Research Foundation (Deutsche Forschungsgemeinschaft-DFG) Collaborative Research Center SFB TRR 40 – “Technological foundations for the design of thermally and mechanically highly loaded components of future space transportation systems”.

References

[1] K. Liang, B. Yang, Z. Zhang, Investigation of heat transfer and coking characteristics of hydrocarbon fuels, Journal of Propulsion and Power, Vol.14, No.5, September-October 1998
[2] P.J. Linstrom and W.G. Mallard, National Institute of Standards and Technology, Gaithersburg MD, 20899, http://webbook.nist.gov, (retrieved October 7, 2016)
[3] H. Burkardt, M. Sippel, A. Herbertz, J. Klevanski, Kerosene vs Methane: A Propellant Tradeoff for reusable Liquid Booster, Journal of Spacecraft and Rockets, Vol. 41, No. 5, September-October 2004
[4] J.M. Locke, S. Pal, R.D. Woodward, Chamber wall heat flux measurements for a LOX/CH4 uni-element rocket, in: 43rd AIAA/ASME/SAE/ASEE Joint Propulsion Conference & Exhibit, 2007, AIAA 2007-5547
[5] O.J. Haidn, M. Oschwald, W. Clauss, etc. LOX/methane Technology Efforts for Future Liquid Rocket Engines, 5th International Spacecraft Propulsion Conference and 2nd International Symposium on Propulsion for Space Transportation, 2008
[6] B. Betti, E. Martelli, F. Nasuti, Heat flux evaluation in oxygen/methane thrust chambers by RANS approach, in: 46th AIAA/ASME/SAE/ASEE Joint Propulsion Conference & Exhibit, 2010, AIAA 2010-6721
[7] S. Ueda, T. Tomita, T. Onodera, Y. Kano, I. Kubota, T. Munenaga,, Hot-Firing Test of Methane-Fueled Rocket Engine under High Altitude Condition, 49th AIAA JPC, AIAA 2013-4056, 2013
[8] A. Kootyev, L. Samoilov, New engines to power advanced Launch Vehicles, Aerospace Journal, May-June 1998
[9] V.P. Zhukov, D.I. Suslov, Measurements and modelling of wall heat fluxes in rocket combustion chamber with porous injector head, Aerospace Science and Technology, 48 (2016) 67–74
[10] P. Tucker, S. Menon, J. Oefelein, V. Yang, C. Merkle, Validation of high-fidelity CFD simulations for rocket injector design, in: 44th AIAA/ASME/SAE/ASEE Joint Propulsion Conference and Exhibit, 2008, AIAA 2008-5226
[11] V.P. Zhukov, Computational fluid dynamics simulations of a GO2/GH2 single element combustor, Journal of Propulsion and Power, 31 (6) (2015) 1707–1714

DOI: 10.13009/EUCASS2017-279

[12] A. Fröhlich, M. Popp, G. Schmidt, D. Thielmann, Heat transfer characteristics of H2/O2 combustion chambers, in: 29th AIAA/ASME/SAE/ASEE Joint Propulsion Conference, 1993, AIAA 93-1826
[13] M.P. Celano, S. Silvestri, G. Schlieben, C. Kirchberger, O.J. Haidn, and O. Knab, Experimental and numerical investigation of GOX-GCH4 shear-coaxial injector element, Progress in Propulsion Physics 8 (2016) 145-164
[14] German Copper Institute, https://www.kupferinstitut.de
[15] J. Lin, J.S. West, R.W. Williams, P.K. Tucker, CFD code validation of wall heat fluxes for a GO2/GH2 single element combustor, in: 41st AIAA/ASME/SAE/ASEE Joint Propulsion Conference & Exhibit, 2005, AIAA 2005-4524
[16] X.W. Wang, G.B. Cai, P. Jin, Scaling of the flow field in a combustion chamber with a gas- gas injector, Chinese Physics B, Vol. 19, No.1 (2010). SCI DOI: 10.1088/1674-1056/19/1/019401
[17] X.W. Wang, P. Jin, G.B. Cai, Method for investigation of combustion flow field characteristics in single-element gas/gas injector chamber, Journal of Beijing University of Aeronautics and Astronautics, 35(9), (2009),1095-1099
[18] P.K. Tucker, S. Menon, C. Merkle, J.C. Oefelein, and V. Yang, An approach to improved credibility of CFD simulations for rocket injector design, in: 43rd AIAA/ASME/SAE/ASEE Joint Propulsion Conference & Exhibit, 2007, AIAA 2007-5572
[19] A. Chemnitz, T. Sattelmayer, C. Roth, O.J. Haidn, Y. Daimon, R. Keller, P. Gerlinger, J. Zips, M. Pfitzner, Numerical Investigation of Flow and Combustion in a Single-Element GCH4/GOX Rocket Combustor: Aspects of Turbulence Modeling, 52nd AIAA/SAE/ASEE Joint Propulsion Conference, Salt Lake City, USA, July 25-27, 2016
[20] Y. Daimon, H. Terashima, H. Negishi, M.P. Celano, S. Silvestri, O.J. Haidn, Combustion Modeling Study for a CH4/GOX single element combustion chamber: Steady State Simulation and Validation, SP2016_3125263, Space Propulsion, Rome 2016
[21] C. Lian, C. Merkle, Contrast between steady and time-averaged unsteady combustion simulations, in: 48th AIAA Aerospace Sciences Meeting Including the New Horizons Forum and Aerospace Exposition, 2010, AIAA 2010-371
[22] I. Yimer, I. Campbell, L.-Y. Jiang, Estimation of the turbulent Schmidt number from experimental profiles of axial velocity and concentration for high-Reynolds-number jet flows, Canadian Aeronautics and Space Journal, 2002, 48(3), 195–200
[23] H. Liu, F. Chen, H. Liu, Z.H. Zheng, S.H. Yang, 18-Step reduced mechanism for methane/air premixed supersonic combustion, Journal of Combustion Science and Technology, 2012, 18(5): 467-472
[24] Fluent Theory Guide, Product Documentation ANSYS Inc. Release 16.2
[25] P. Beck, B. Wagner, O. Haidn, The influence of secondary flows in the thrust acting on the axis of a radial Lox pump, 12th European Conference on Turbomachinery Fluid dynamics & Thermodynamics, 2017, 2017-04
[26] B. J. McBride, and S. Gordon, Computer program for calculation of complex equilibrium compositions and applications, NASA Reference Publication, 1311, 1996
[27] C. Roth, O. Haidn, A. Chemnitz, T. Sattelmayer, Y. Daimon, G. Frank, H. Müller, J. Zips, M. Pfitzner, R. Keller, P. Gerlinger, D. Maestro, B. Cuenot, H. Riedmann, L. Selle, Numerical Investigation of Flow and Combustion in a Single-Element GCH4/GOX Rocket Combustor, 52nd AIAA/SAE/ASEE Joint Propulsion Conference, Salt Lake City, USA, July 25-27, 2016
[28] D. Maestro, B. Cuenot, L. Selle, G. Frank, M. Pfitzner, Y. Daimon, R. Keller, P. Gerlinger, A. Chemnitz, T. Sattelmayer, O. Haidn, Numerical Investigation of Flow and Combustion in a Single-Element GCH4/GOX Rocket Combustor : Chemistry Modeling and Turbulence-Combustion Interaction, 52nd AIAA/SAE/ASEE Joint Propulsion Conference, Salt Lake City, USA, July 25-27, 2016